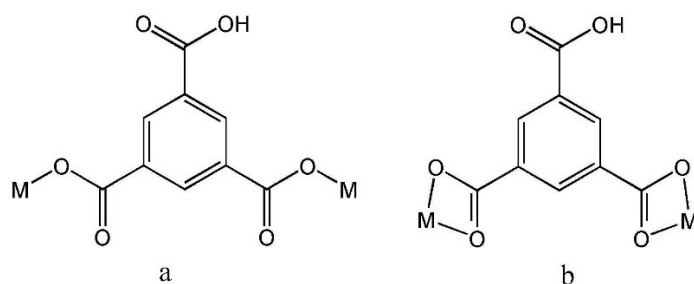


Supporting Information

Ratiometric Fluorescence Determining the Anthrax Biomarker 2,6-Dipicolinic Acid by $\text{Eu}^{3+}/\text{Tb}^{3+}$ -doped Nickel Coordination Polymer

Hang Lei, Cui-Xing Qi, Xuan-Bo Chen, Tian Zhang, , Ling Xu* and Bing Liu*



Scheme S1. The coordination fashions of HBTC²⁻ ligands in Ni-BTC.

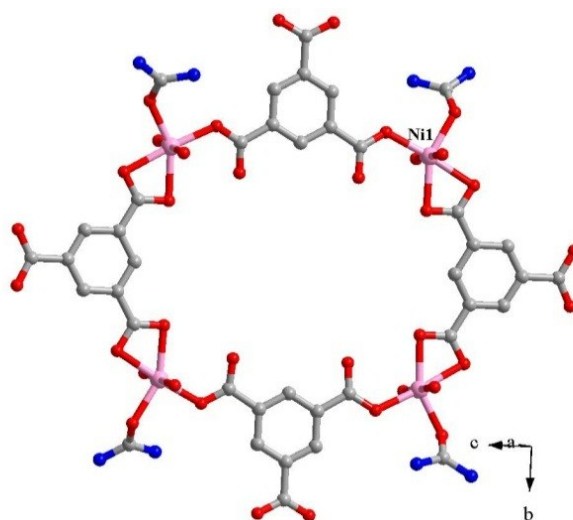


Fig. S1. The structure motif of discrete Ni-BTC with 32-membered ring.

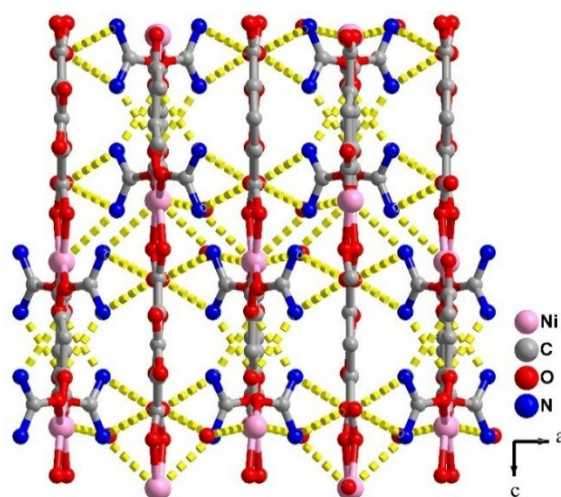


Fig. S2. The 3D supramolecular framework of Ni-BTC constructed by H-bondings.

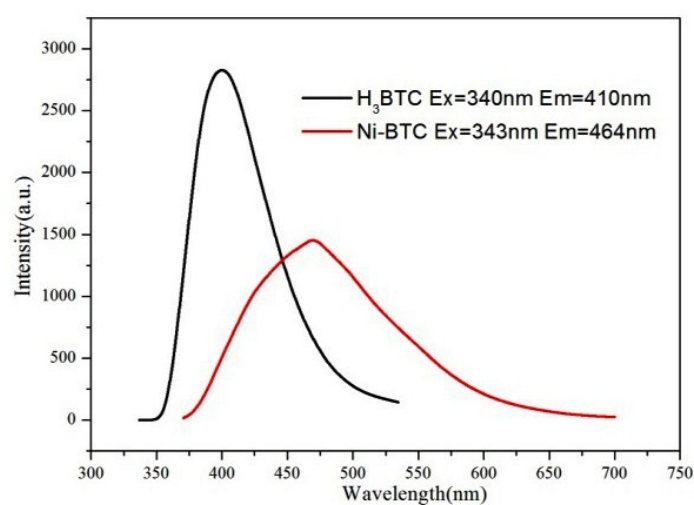


Fig. S3. The solid-state emission spectra of free H₃BTC ligand with $\lambda_{\text{ex}} = 340$ nm and Ni-BTC with $\lambda_{\text{ex}} = 343$ nm.

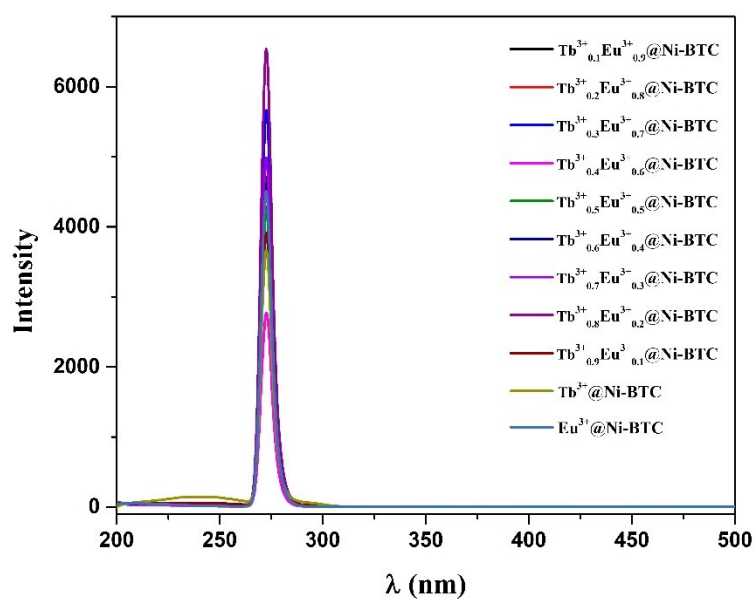


Fig. S4. The excitation spectra of $\text{Tb}^{3+}/\text{Eu}^{3+}@/\text{Ni-BTC}$ composites with comparison of that of $\text{Tb}^{3+}@/\text{Ni-BTC}$ and $\text{Eu}^{3+}@/\text{Ni-BTC}$.

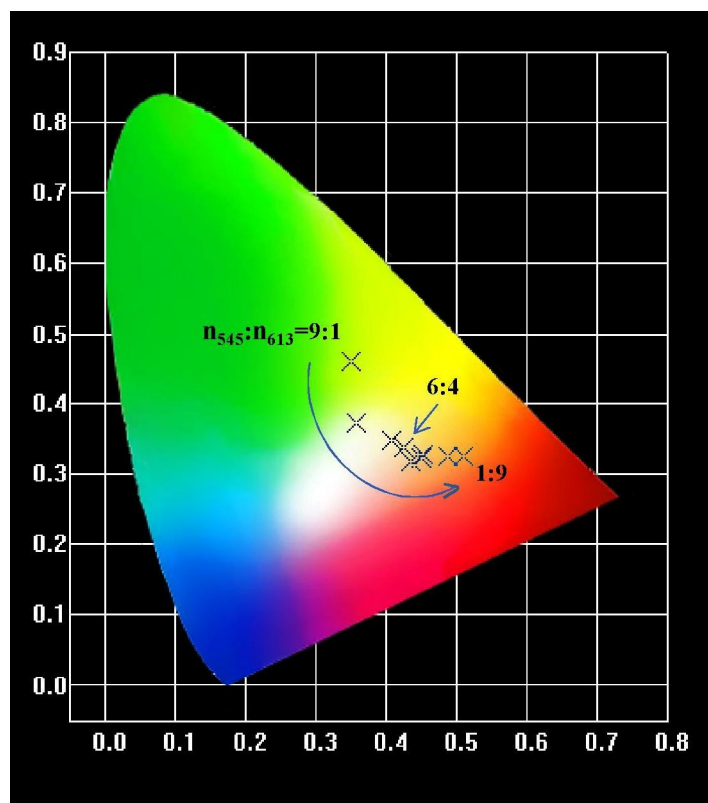


Fig. S5. The CIE 1931 chromaticity diagram together with the calculated color coordinate of $\text{Tb}^{3+}/\text{Eu}^{3+}@/\text{Ni-BTC}$ composites.

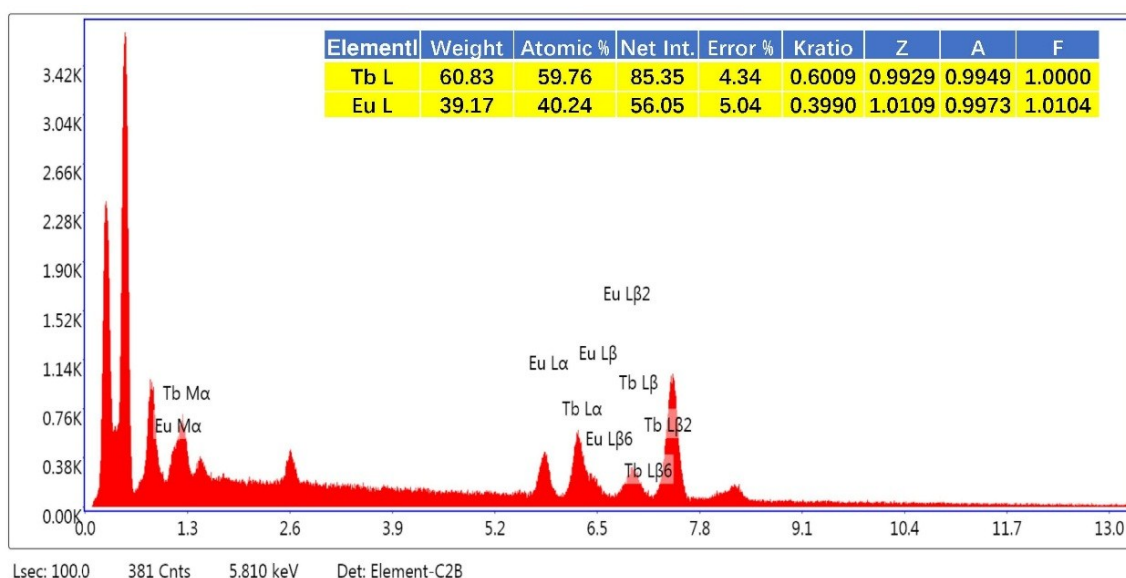


Fig. S6. EDS of Tb^{3+} and Eu^{3+} in $\text{Tb}^{3+}_{0.6}/\text{Eu}^{3+}_{0.4}@/\text{Ni-BTC}$.

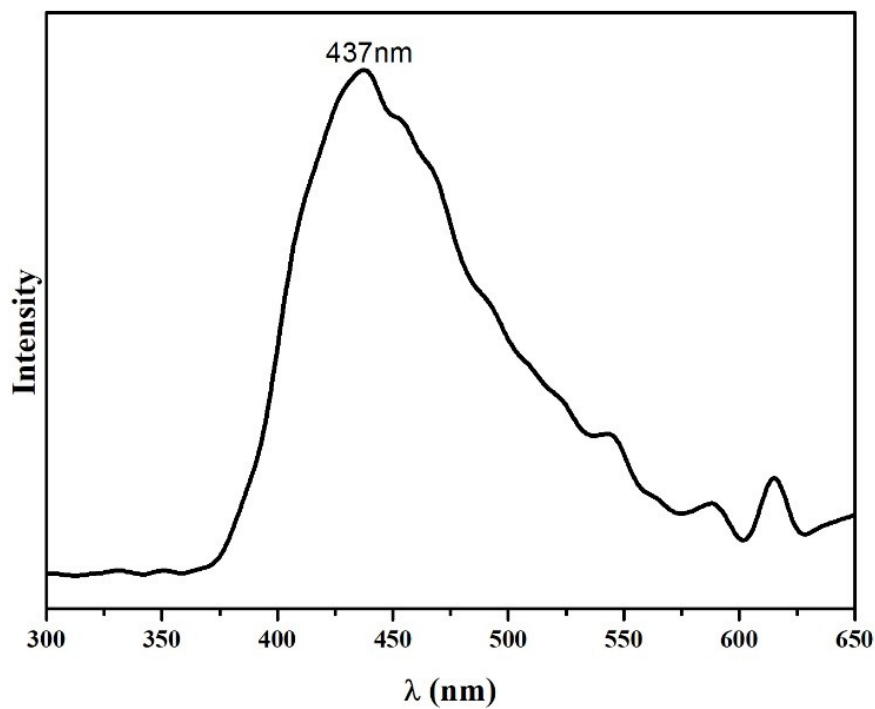


Fig. S7. The low-temperature phosphorescence spectrum of Gd-BTC under 270 nm excitation at 77 K.

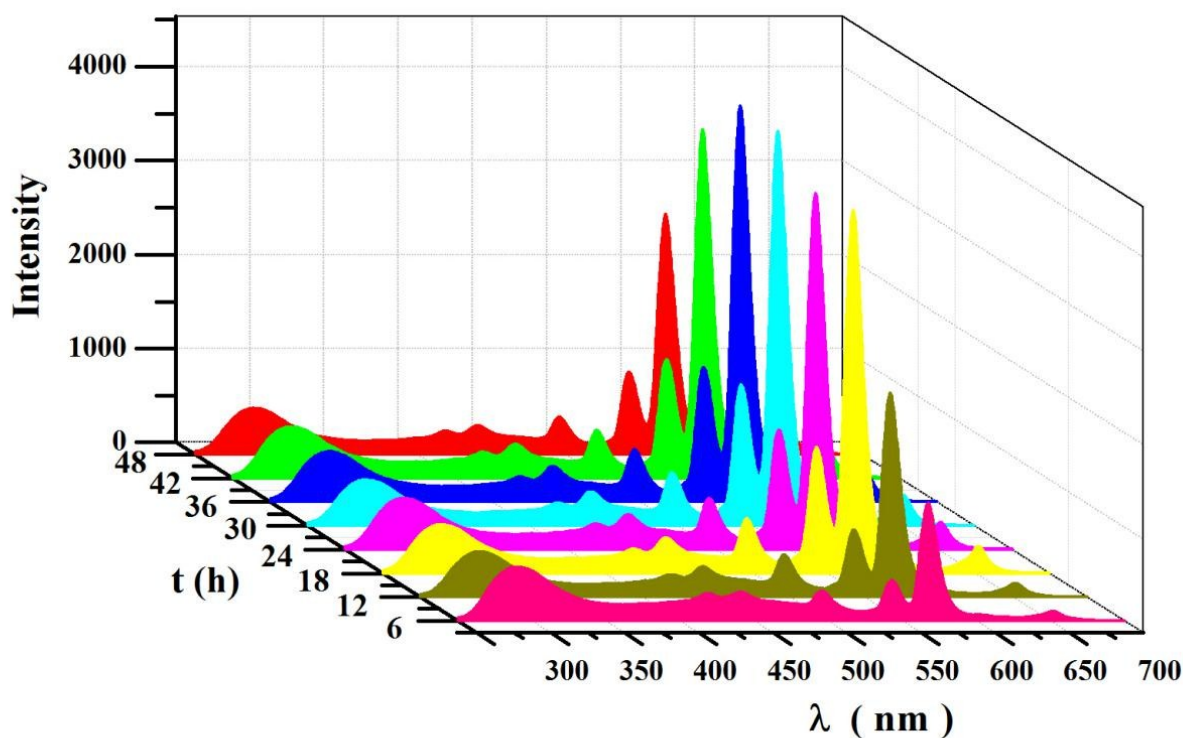


Fig. S8. The solid-state emission spectra of $\text{Tb}^{3+}_{0.6}/\text{Eu}^{3+}_{0.4}@\text{Ni-BTC}$ ($\lambda_{\text{ex}} = 270 \text{ nm}$) with soaking time of 6-42 h recorded at ambient temperature.

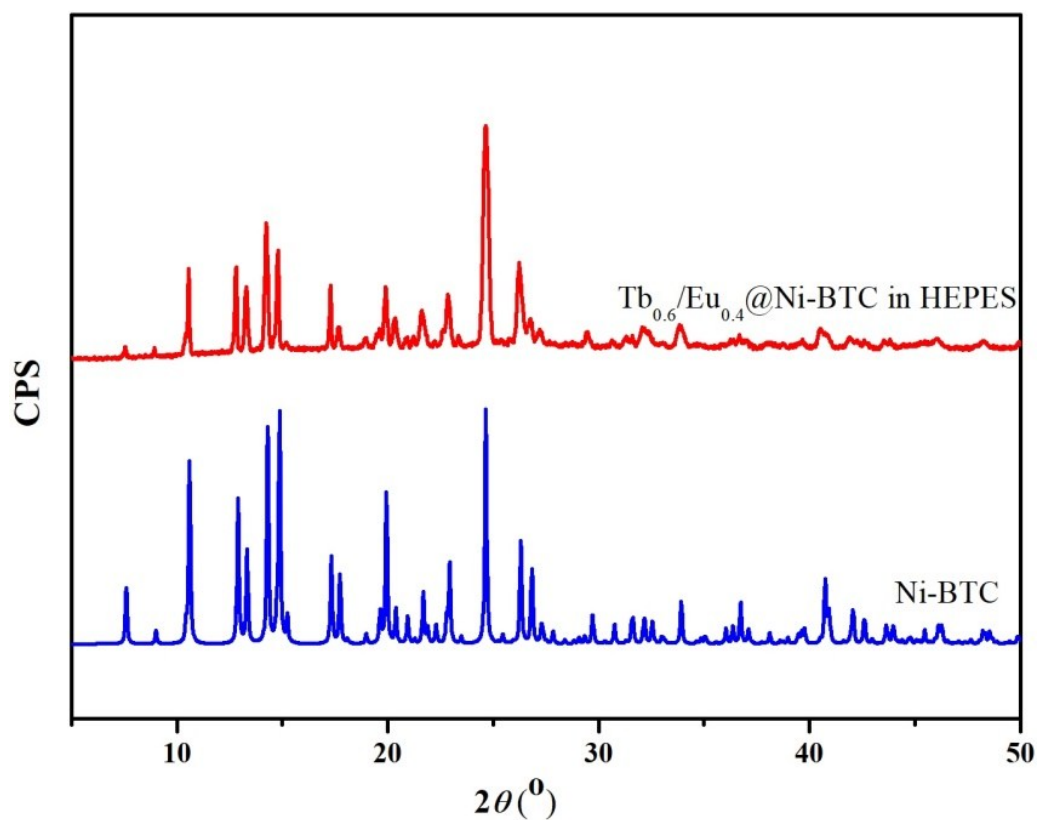


Fig. S9 The PXRD patterns of Ni-BTC and $\text{Tb}^{3+}_{0.6}/\text{Eu}^{3+}_{0.4}@\text{Ni-BTC}$ dispersed in HEPES buffer solution.

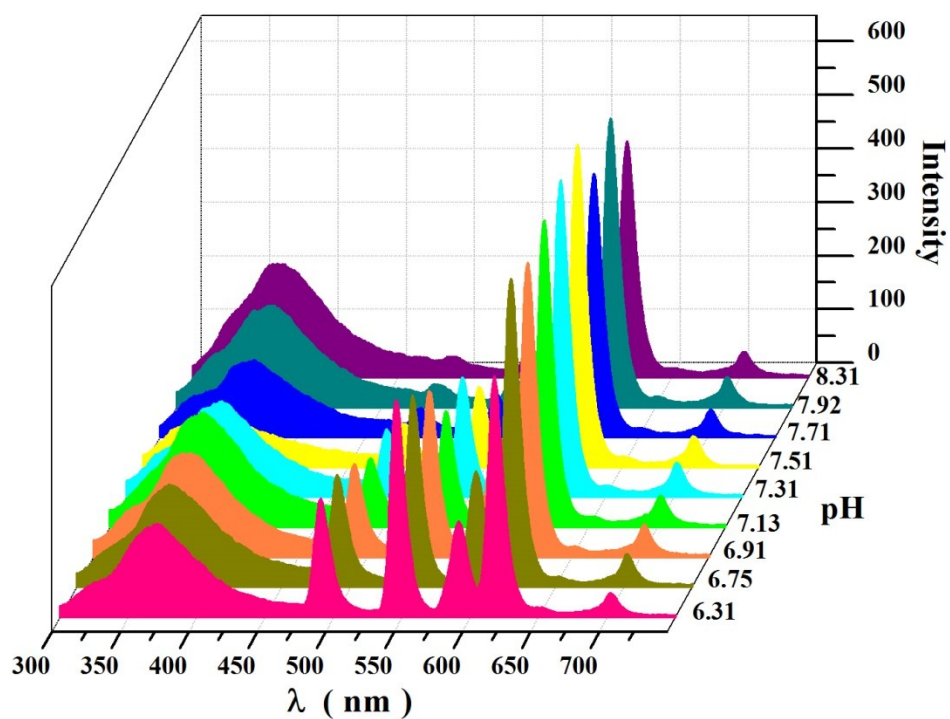


Fig. S10. The solid-state emission spectra of $\text{Tb}^{3+}_{0.6}/\text{Eu}^{3+}_{0.4}@\text{Ni-BTC}$ ($\lambda_{\text{ex}} = 270 \text{ nm}$) without DPA added depending on pH recorded at ambient temperature.

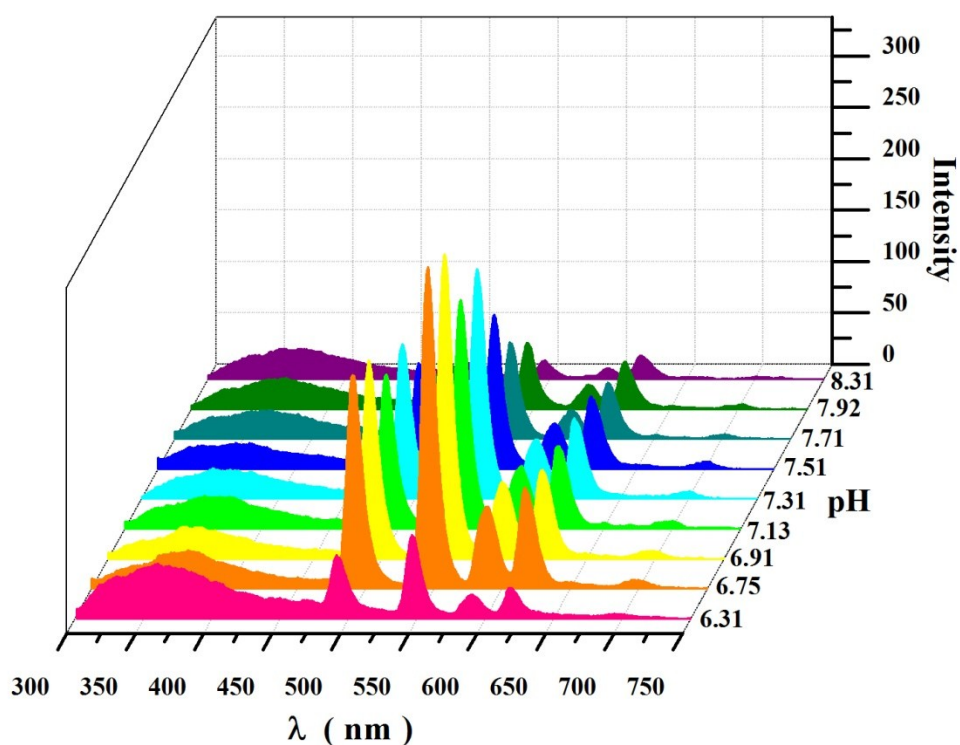


Fig. S11. The solid-state emission spectra of $\text{Tb}^{3+}_{0.6}/\text{Eu}^{3+}_{0.4}@\text{Ni-BTC}$ ($\lambda_{\text{ex}} = 270 \text{ nm}$) with DPA added depending on pH values recorded at ambient temperature.

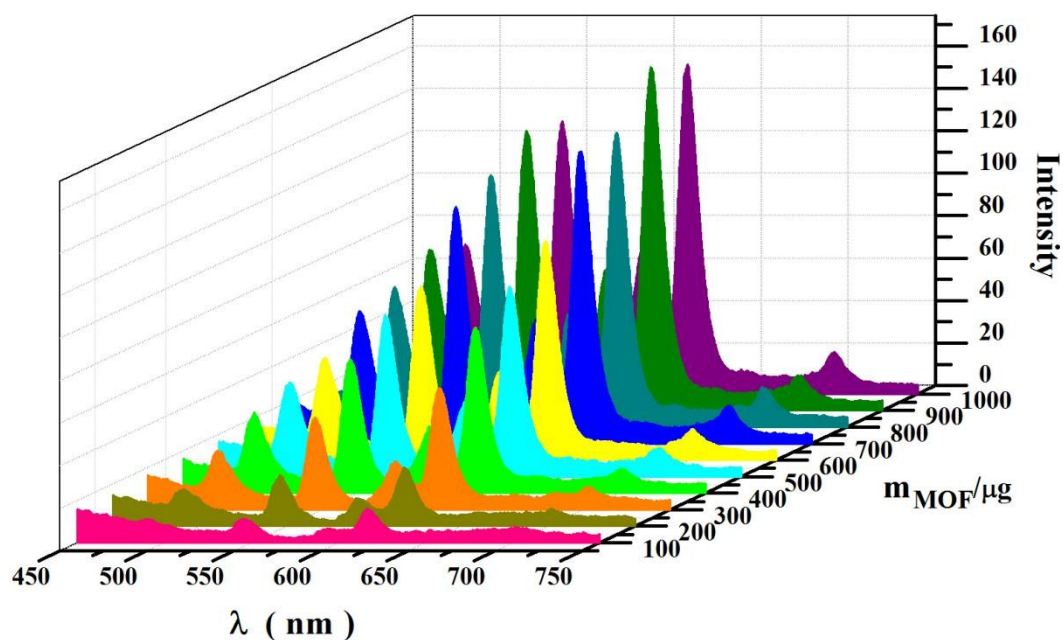


Fig. S12. The solid-state emission spectra of $\text{Tb}^{3+}_{0.6}/\text{Eu}^{3+}_{0.4}@\text{Ni-BTC}$ ($\lambda_{\text{ex}} = 270 \text{ nm}$) without DPA dropped depending on the dosage of $\text{Tb}^{3+}_{0.6}/\text{Eu}^{3+}_{0.4}@\text{Ni-BTC}$ recorded at ambient temperature.

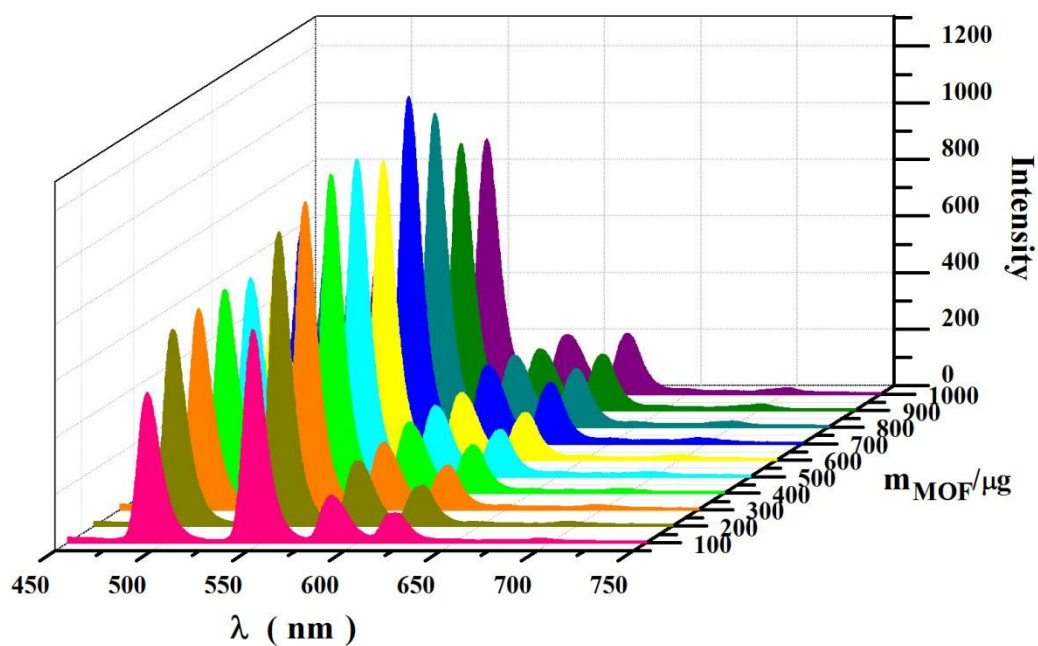


Fig. S13. The solid-state emission spectra of $\text{Tb}^{3+}_{0.6}/\text{Eu}^{3+}_{0.4}@ \text{Ni-BTC}$ ($\lambda_{\text{ex}} = 270$ nm) dropped with DPA depending on the dosage of $\text{Tb}^{3+}_{0.6}/\text{Eu}^{3+}_{0.4}@ \text{Ni-BTC}$ recorded at ambient temperature.

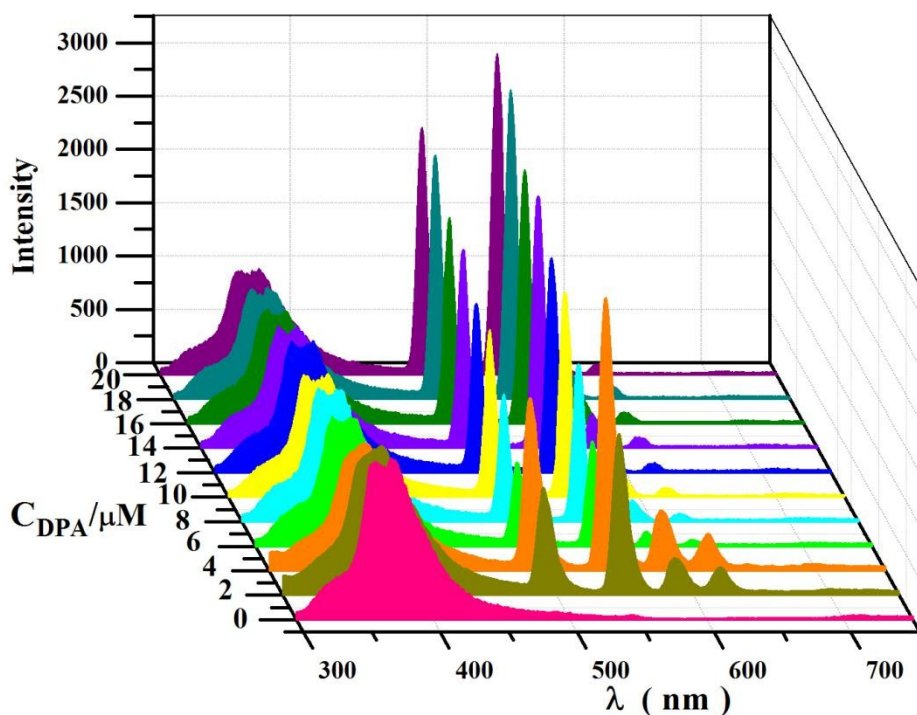


Fig. S14. The solid-state emission spectra of $\text{Tb}^{3+}_{0.6}/\text{Eu}^{3+}_{0.4}@ \text{Ni-BTC}$ ($\lambda_{\text{ex}} = 270$ nm) depending on C_{DPA} of 0-20 $\mu\text{mol/L}$ recorded at ambient temperature.

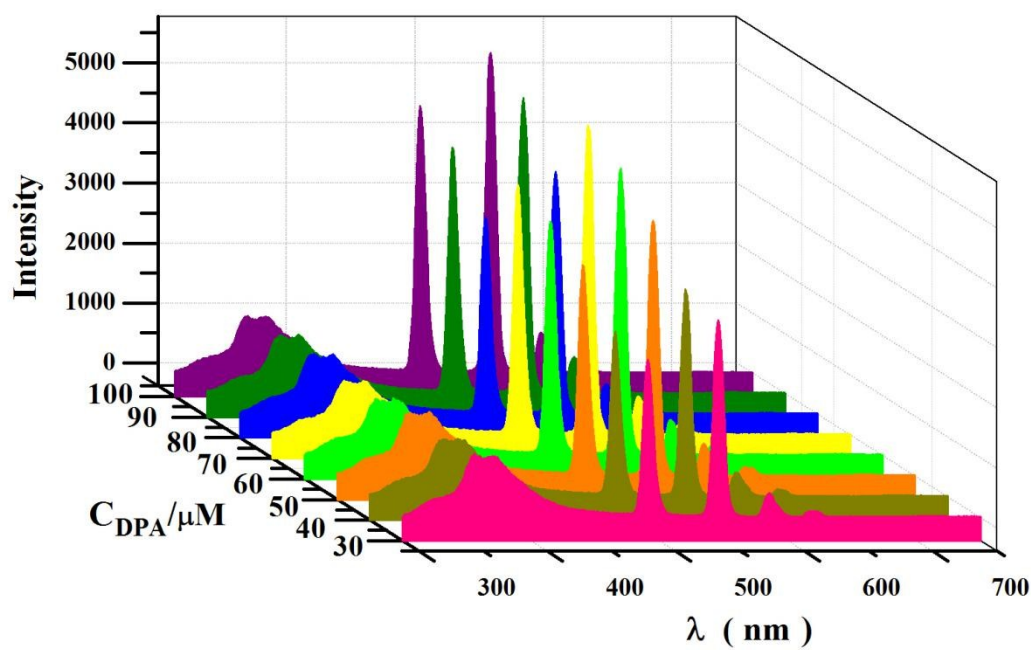


Fig. S15. The solid-state emission spectra of Tb³⁺_{0.6}/Eu³⁺_{0.4}@Ni-BTC ($\lambda_{\text{ex}} = 270$ nm) depending on C_{DPA} of 30-100 $\mu\text{mol/L}$ recorded at ambient temperature.